ACS Chemical Neuroscience

Research Article

pubs.acs.org/chemneuro

Glyconanoparticle Aided Detection of β-Amyloid by Magnetic Resonance Imaging and Attenuation of β-Amyloid Induced Cytotoxicity

Hovig Kouyoumdjian,[†] David C. Zhu,[‡] Mohammad H. El-Dakdouki,[†,∥] Kelly Lorenz,[†] Jianjun Chen,[§] Wei Li,[§] and Xuefei Huang*[,†]

[†]Department of Chemistry, 578 S. Shaw Lane, Room 426, Michigan State University, East Lansing, Michigan 48824, United States

[‡]Departments of Radiology and Psychology, Michigan State University, East Lansing, Michigan 48824, United States

[§]Department of Pharmaceutical Sciences, College of Pharmacy, University of Tennessee Health Science Center, 847 Monroe Avenue, Memphis, Tennessee 38163, United States

Supporting Information

ABSTRACT: The development of a noninvasive method for the detection of Alzheimer's disease is of high current interest, which can be critical in early diagnosis and in guiding treatment of the disease. The aggregates of β-amyloid are a pathological hallmark of Alzheimer's disease. Carbohydrates such as gangliosides have been shown to play significant roles in initiation of amyloid aggregation. Herein, we report a biomimetic approach using superparamagnetic iron oxide glyconanoparticles to detect β-amyloid. The bindings of β-amyloid by the glyconanoparticles were demonstrated through several techniques including enzyme linked immunosorbent assay, gel electrophoresis, tyrosine fluorescence assay, and transmission electron microscopy. The superparamagnetic nature of the nanoparticles allowed easy detection of β-amyloid both in vitro and ex vivo by magnetic resonance imaging. Furthermore, the glyconanoparticles not only were nontoxic to SH-SY5Y neuroblastoma cells but also greatly reduced β-amyloid induced cytotoxicity to cells, highlighting the potential of these nanoparticles for detection and imaging of β-amyloid.

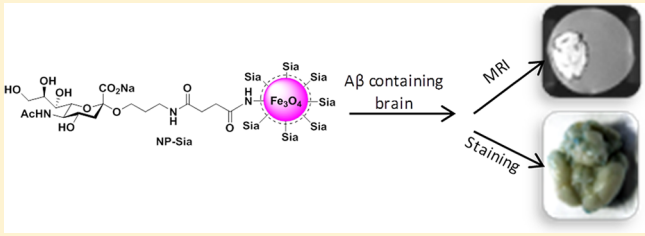

KEYWORDS: *β-Amyloid, carbohydrates, cytotoxicity, magnetic glyconanoparticles, magnetic resonance imaging*

Alzheimer's disease (AD) is a progressive degenerative disease characterized by the destruction of nerve cells and neural connections in the cerebral cortex. In 2011, 5.4 million people in the United States had AD with an estimated cost of $183 billion in medical care.[1] It is forecasted that the number of AD patients and medical care cost will triple by 2050.[2] These staggering numbers suggest the urgent need to better understand, diagnose, and treat AD. Traditional diagnostic approaches toward AD rely on the analysis of cognitive abilities and behavior of patients, which are nonspecific and prone to false results. Neuroimaging using magnetic resonance imaging (MRI),[3] single photon emission computed tomography (SPECT), or positron emission tomography (PET) has become an important tool to aid in AD detection.[4] These techniques can provide important information on morphological and functional changes of brain, which are more suitable toward imaging advanced stages of AD.

For early detection of AD before any clinical manifestation, biomarker-detection based strategies are gaining momentum. Although the etiology of AD is not yet well understood, β-amyloid peptide (Aβ), the major constituent of amyloid plaques, is one of the most prominent pathological hallmarks of AD.[5] Aβ peptide is produced by proteolytic cleavage of the amyloid precursor protein in the central nervous system by β- and γ-secretases. Although Aβ can contain varying numbers of amino acids ranging from 36 to 42, the most abundant forms are Aβ(1−40) and Aβ(1−42).[6] Aβ is prone to aggregation to form plaques, and the extra two hydrophobic residues in the C-terminus of Aβ(1−42) render it aggregate faster than Aβ(1−40).[7]

Due to its important role in AD, Aβ imaging has been actively pursued in vivo using noninvasive techniques including PET,[8] MRI,[9] and near IR fluorescence imaging.[10] Multiple PET reagents that can selectively bind with Aβ have been developed for determination of plaque burden in human patients with several undergoing late stage clinical trials.[8] Although PET can give high sensitivities, MRI is a complementary approach due to its high spatial and temporal resolution. Furthermore, MRI does not require ionizing radiation thus is suitable for longitudinal studies. To better detect Aβ by MRI, MRI contrast agents have been developed using full length or fragments of Aβ as targeting ligands.[9a−c] As Aβ has the inherent affinity with amyloid plaques, these targeted agents could selectively bind

Received: November 8, 2012
Accepted: January 7, 2013
Published: January 8, 2013

with amyloid plaques, thus enhancing the contrast from surrounding tissues and enabling plaque visualization by MRI. In addition to the usage of Aβ peptide, ground breaking ^{19}F-MRI studies have been performed using a fluorine-containing Congo red derivative to image amyloid plaques in mice.[9e] Besides these targeted versions of contrast agents, a nonspecific commercially available gadolinium based agent was explored for Aβ imaging by intracerebroventricular injection.[9d] Presumably due to the hydrophobicity of the Aβ plaques, the hydrophilic gadolinium agent avoided Aβ plaques while staining the rest of the brain well, thus enhancing the contrast between Aβ plaques and surrounding tissues. These innovative studies have revealed the potential power of MRI for Aβ imaging and continual development of contrast agents is necessary to realize the full potential of this technique.

Due to the ubiquitous existence of carbohydrates, they can influence Aβ aggregation. Glyco-conjugates including gangliosides and anionic glyco-polymers (e.g., glycosaminoglycans and nucleic acids) have been reported to bind Aβ.[11] Gangliosides such as GM1 (a sialic acid containing glycosphingolipid)[12] are abundant in neuronal plasma membranes and involved in synaptic signaling and transmission.[13] GM1-bound Aβ has been found in the brains of AD patients,[12a] with GM1 shown to serve as nucleation sites on neuronal cell membrane for Aβ aggregation.[12c] The negatively charged sialic acid moiety of GM1 is critical for Aβ interactions[14] through hydrogen bonding with His13, and clustering of sialic acid can significantly enhance the binding with Aβ.[14,15] Based on these findings, we became interested in exploring whether carbohydrates can be utilized for Aβ detection and imaging.

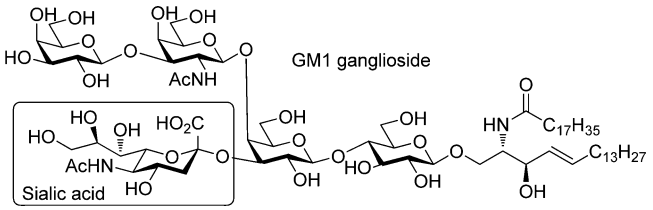

Nanotechnology has been introduced to Aβ research with the majority of the studies focusing on the effects of nanoparticles on Aβ aggregation.[16] The nanoparticle platform is very useful for our study, as it can display multiple copies of ligands that can potentially interact with Aβ leading to enhanced avidity. Herein, we report the development of magnetic glyconanoparticles, where the magnetic cores of the nanoparticles are coated with carbohydrates. The glyconanoparticles can selectively bind with Aβ and the magnetic properties of these nanoparticles enable the Aβ detection in vitro and ex vivo by MRI. Furthermore, these nanoparticles can expedite the aggregation of Aβ and mitigate Aβ induced cellular toxicity.

RESULTS AND DISCUSSION

Preparation and Characterization of NP-Sia. Our study started from the synthesis of magnetic glyconanoparticles with magnetite (Fe_3O_4) cores. The superparamagnetic magnetite nanoparticles (SPIONs) were prepared by coprecipitating ferric chloride and ferrous sulfate under basic condition in the presence of the polysaccharide dextran (Figure 1a).[17] Dextran coats the external surface of the nanoparticles forming a stable colloidal suspension. Dextran coating was cross-linked with epichlorohydrin, which was followed by ammonia treatment to introduce amine groups (SPION-NH_2). Sialic acid methyl ester derivative **1**[18] was partially deprotected under the Zemplén condition producing sialic acid **2**, which was subsequently linked to SPION-NH_2 via amide coupling mediated by 1-ethyl-3-(3-dimethylaminopropyl) carbodiimide (EDC) (Figure 1b). The methyl ester of sialic acid was removed by saponification leading to sialic acid coated NPs (NP-Sia).

NP-Sia was characterized via a variety of techniques, including transmission electron microscopy (TEM), high-resolution magic angle spinning nuclear magnetic resonance (HRMAS NMR), thermogravimetric analysis (TGA), zeta potential, dynamic light scattering (DLS), thiobarbituric acid assay (TBA), and MRI (Figure 1 and Supporting Information Figure S1). TEM images indicated that the diameters of NP core were around 5 nm (Figure 1c). Both SPIONs and NP-Sia have close to neutral zeta potentials in PBS buffer (−1.8 and 2.5 mV, respectively). The total carbohydrate content represented 80% weight of NP-Sia as determined by TGA (Figure S1a). To analyze the amount of sialic acid on NPs, sialic acid was selectively cleaved under a mild acidic condition and the amount of sialic acid was quantified by TBA showing that sialic acid accounted for 4% weight of the NPs (Figures S1b, Supporting Information). This suggests on average there are 98 copies of sialic acid on each NP. The presence of dextran and sialic acid was also confirmed by HRMAS NMR with their characteristic chemical shifts observed in ^{1}H NMR spectrum of the NP-Sia (Supporting Information Figure S1c). The NP-Sia is an excellent contrast agent with high magnetic relaxivity. (The R2* magnetic relaxation rate (R2* = 1/T2*) of NP-Sia was measured to be 143 mM^{-1} s^{-1} at 3T (Figure 1d). The R1 and R2 values for NP-Sia were 3.5 and 198 mM^{-1} s^{-1}, respectively, as shown in Supporting Information Figure S1d,e.)

Assessment of NP-Sia Binding with Aβ via ELISA and Prussian Blue Staining. In order to study NP interactions with Aβ, we selected Aβ(1−42), since it is a major component of amyloid peptides in the senile plaques in AD brains[19] and it is considered the most toxic Aβ forms.[20] The Aβ peptide was dissolved in 10 mM NaOH solution, which was diluted in PBS buffer to the desired final concentration. The Aβ monomer solution was incubated at 37 °C for 48 h without stirring to form fibrils. To check the quality of the fibrils, thioflavin (ThT) binding assay was performed. ThT is a cationic benzothiazole salt, which displays enhanced fluorescence and a characteristic red shift of its emission maximum when bound with β-sheet structures.[21] Upon incubation of Aβ fibrils with ThT, significant enhancement of ThT fluorescence and red shift of its emission (489 nm) were observed suggesting that good quality β-sheet rich Aβ fibrils were obtained (Supporting Information Figure S2a).[22] TEM imaging also showed fibrillar structures of Aβ (Supporting Information Figure S2b). In order to visualize Aβ in TEM, 2% uranyl acetate stain on the fibril was needed to provide contrast from the background.

The interactions between NP-Sia and Aβ fibril were investigated first using an enzyme-linked immunosorbent assay (ELISA). A solution of NP-Sia was added to a microtiter plate. After overnight incubation, NPs adhered to the bottom of the wells. Aβ solutions were added to the NP-Sia coated wells followed by thorough washing and addition of an anti-Aβ IgG primary antibody. The amount of Aβ bound was quantified by the absorbance change of each well upon incubation with an anti-IgG secondary antibody linked with horse radish peroxidase (HRP). As shown in Figure 2a, a dose dependent increase in absorbance was observed with increasing Aβ

dx.doi.org/10.1021/cn3002015 | ACS Chem. Neurosci. 2013, 4, 575−584

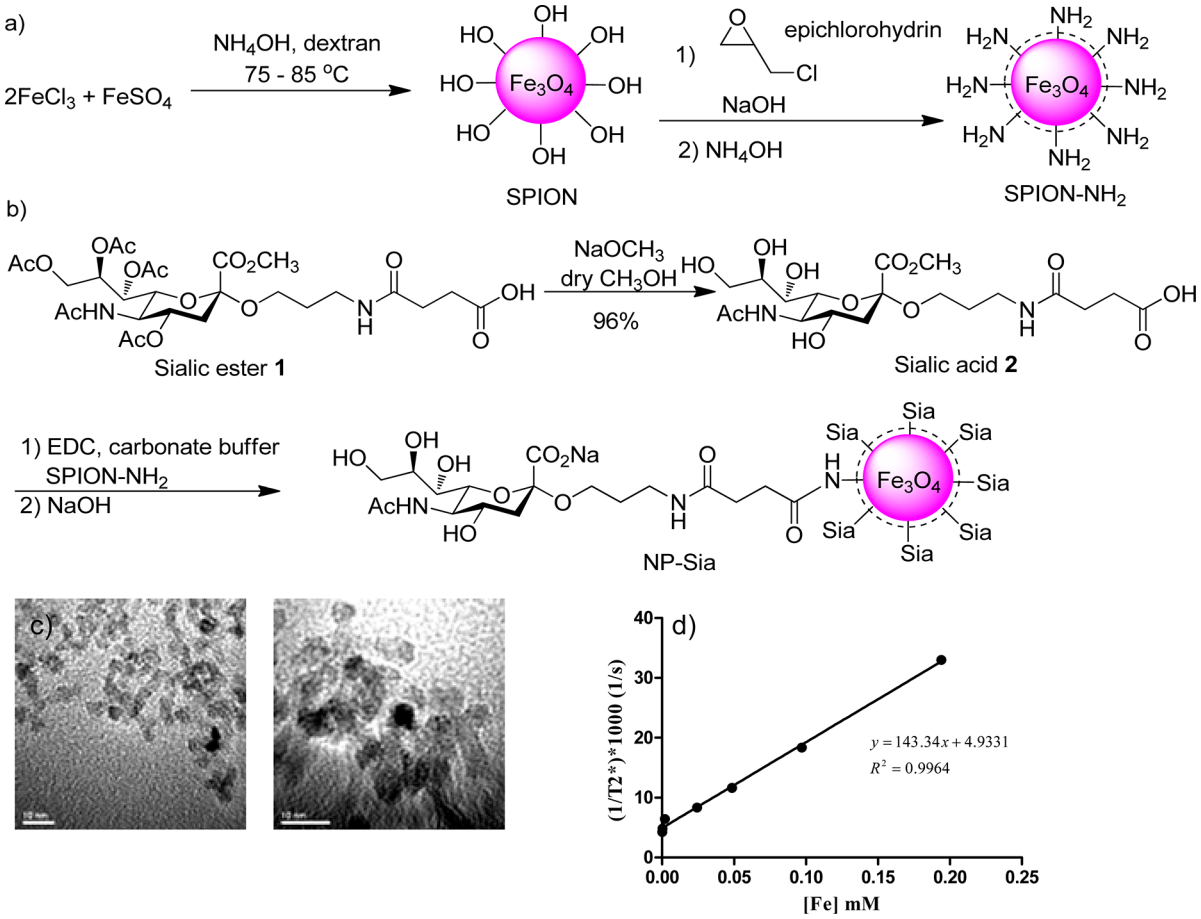

Figure 1. Synthesis of (a) SPION and (b) NP-Sia. (c) TEM (scale bar is 10 nm) and (d) T2* relaxivity characterization of NP-Sia.

concentration (apparent K_d = 0.7 μM). The immobilization of NP-Sia on the plate was important for Aβ binding, as without NP coating, the absorbance of Aβ on naked plates was much lower after washing (Figure 2a). Although the dextran coated SPION could be recognized by Aβ presumably due to its negative surface charges,[23] the addition of sialic acid onto the dextran NP (NP-Sia) enhanced NP binding with Aβ (Supporting Information Figure S3a). To further ascertain the role of sialic acid, a competitive ELISA was performed when fixed amount of Aβ was added to NP-Sia coated plates together with free sialic acid. As free sialic acid should compete with NP-Sia for Aβ binding, the amount of Aβ remained on the plate should decrease with increasing amount of sialic acid. This was observed experimentally (Figure 2b), supporting the notion that sialic acid plays a considerable role in mediating Aβ binding.[14]

In ELISA, blocking agents such as bovine serum albumin (BSA) is commonly employed to reduce the nonspecific adsorption of proteins on the microtiter plate, including some for Aβ binding studies.[24] However, in our assays, we observed a considerable difference between the BSA-blocked and unblocked wells, where the wells incubated with BSA showed significantly higher Aβ binding even without any NP present compared to those not containing BSA (Supporting Information Figure S3b). Varying the amount of BSA (0.1−5%) as well as using milk as the blocking agent did not resolve this problem. We attributed this to the adsorption of Aβ by BSA or milk proteins. This outcome was in agreement with a report showing the strong affinities of plasma proteins such as albumin with Aβ,[25] suggesting the importance of protein free blocking in ELISA for Aβ detection.

To further prove the binding between Aβ and NP-Sia, we performed Prussian blue staining, which is a staining method specific for iron. NP-Sia by itself could bind to the 24-well cell culture plate, which was evident from the bright blue color when Prussian blue reagent was added to wells incubated with NP-Sia (Figure 3a). If Aβ binds with free NP-Sia, the Aβ/NP-Sia complex should have reduced adhesion to the microtiter plate due to shielding of NP-Sia by Aβ. Indeed, when NP-Sia was preincubated with Aβ fibril (25 μM) and then added to the plate followed by washing, much reduced blue color was observed with Prussian blue staining (Figure 3b). Higher concentration of Aβ (100 μM) further decreased the level of Prussian blue (Figure 3c). Aβ by itself did not bind much with the wells under the experimental conditions. These observations support the conclusion that NP-Sia can bind with Aβ.

Confirmation of Aβ and NP-Sia Binding by Tyrosine Fluorescence Measurement and TEM. Aβ contains a tyrosine residue (Tyr10), the intrinsic fluorescence of which can be used to monitor binding.[24d] Aβ monomer (30 μM) was incubated with various concentrations of NP-Sia (0.02, 0.2, and 2 mg/mL) at room temperature. After 24 h, the solution was centrifuged and the tyrosine fluorescence of the supernatant was recorded (Figure 4a). Centrifugation of Aβ or NP-Sia alone at 10 000g did not produce any pellets or fluorescence changes. However, incubation of Aβ with NP-Sia followed by centrifugation showed a dose dependent decrease of supernatant fluorescence. The fluorescence intensity dropped to

dx.doi.org/10.1021/cn3002015 | ACS Chem. Neurosci. 2013, 4, 575−584

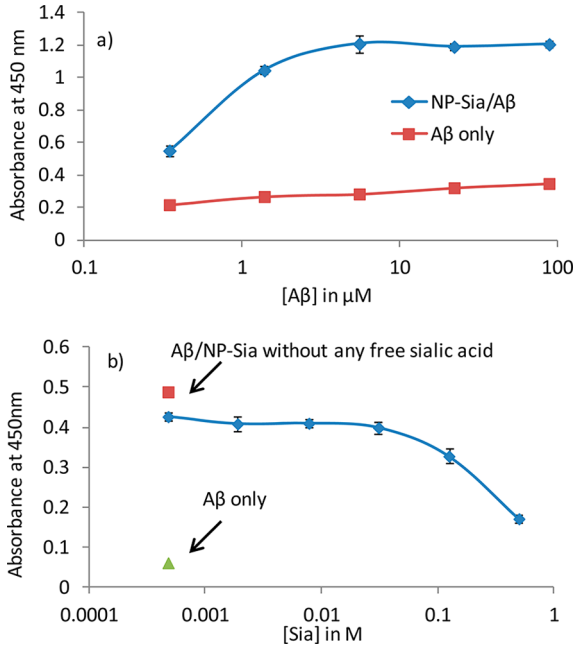

Figure 2. (a) ELISA curve for Aβ binding to immobilized NP-Sia); (b) ELISA curve of Aβ (0.5 μM) binding to immobilized NP-Sia in the presence of increasing concentration of free sialic acid (blue circle). For comparison, the absorbance of wells containing Aβ (0.5 μM) binding to immobilized NP-Sia without any free sialic acid (red square) and Aβ (0.5 μM) binding to bare wells (green triangle) are also shown. The error bars in all graphs represent the standard deviation of four wells.

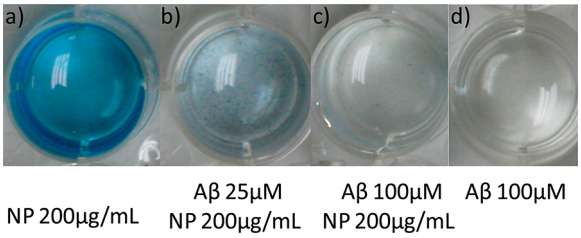

Figure 3. Pictures of 24-well cell culture plates after incubation with (a) NP-Sia (200 μg/mL); (b) NP-Sia (200 μg/mL) incubated with Aβ (25 μM); (c) NP-Sia (200 μg/mL) incubated with Aβ (100 μM); and (d) Aβ (100 μM). After thorough washing, the wells were treated with Prussian blue.

baseline levels with 2 mg/mL NP-Sia, suggesting complete removal of Aβ from the solution. A pellet was observed at the bottom in tubes where NP-Sia was incubated with Aβ, indicating that NP-Sia formed aggregates with Aβ. The binding between NP-Sia and Aβ was confirmed by TEM of the pellets (Figure 4b–d). Unlike free Aβ, it was not necessary to add uranyl acetate to stain Aβ since the NP bound provided sufficient contrast in TEM. Extensive aggregates were evident from TEM images with higher concentrations of NP-Sia (Figure 4b–d).

NP-Aβ Binding Detected by MRI. Due to their high magnetic relaxivities, the superparamagnetic nanoparticles are useful contrast agents for T2/T2* based MR imaging.[26] Another interesting property of the magnetic nanoparticles is that their transverse relaxivities can be significantly enhanced when they form larger clusters due to target binding.[18a,27] This magnetic relaxation switching phenomenon has been utilized for biological detections.[18a,27] As supported by our tyrosine fluorescence and TEM studies discussed above, we envision the multivalent binding of NP-Sia with Aβ should lead to the formation of NP clusters. These clusters can create larger local magnetic field inhomogeneities thus are more efficient in dephasing the spins of surrounding water protons and lowering T2* relaxation time.

The binding of Aβ fibril with NP-Sia was examined by MRI. After incubation of Aβ with NP-Sia (0.1 mg/mL) overnight at room temperature, T2* weighted MR images were acquired. The presence of Aβ led to many more darkened spots compared to NP-Sia alone enabling the detection of Aβ (Figure 5a vs c). Quantification of the images demonstrated that the T2* relaxation time of NP-Sia (0.1 mg/mL) was 23 ms, which was reduced to 16 ms in the presence of Aβ (Figure 5e). Addition of 0.1 M free sialic acid during incubation significantly reduced the number of dark spots in T2* weighted images, presumably due to the competitive binding of free sialic acid to Aβ (Figure 5b,e). This was corroborated by the increase in T2* relaxation time (20 ms). Similar phenomena were observed when Aβ monomer was incubated with NP-Sia (Supporting Information Figure S4).

In another experiment, increasing concentrations of Aβ were incubated with a fixed amount of NP-Sia (0.1 mg/mL). Higher Aβ concentration should lead to more extensive NP-Sia aggregation and reduction of T2* relaxation time, which was observed experimentally (Figure 5f). The limit of detection was 0.05 μM Aβ in this experiment.

Ex Vivo Detection of Aβ by NP-Sia Aided MRI. To test the selectivity of NP-Sia in tissue binding and lay the foundation for future in vivo applications, we examined ex vivo detection of Aβ by NP-Sia in a mouse brain. Brains were harvested from C57BL6 mice and incubated in a solution of Aβ fibrils for 48 h. Aβ was absorbed on the surface of the brains, and the unbound Aβ was removed by thorough washing. The Aβ containing brains were then treated with NP-Sia followed by removal of unbound particles. T2* weighted MR images were acquired, and dark spots were observed on the surface of Aβ brains incubated with NP-Sia (Figure 6a). The dark spots on the surface disappeared when free sialic acid was added during incubation to compete with NP-Sia binding (Figure 6b). As a control, Aβ brain without NP incubation or normal mouse brain incubated with NP-Sia was imaged using the same MRI protocol. No darkening of the brain surface was observed in these cases (Figure 6c, d). Furthermore, Prussian blue staining showed that only Aβ brains incubated with NP-Sia exhibited the characteristic blue color due to the presence of iron (Figure 6e), whereas the other brains (normal brain + NP-Sia, Aβ brain, Aβ brain + NP-Sia + free sialic acid) showed little blue coloration (Figure 6f–h), thus supporting MRI results. These observations suggest that NP-Sia did not nonspecifically bind with brain components and Aβ could be detected by NP-Sia aided MRI in this ex vivo model.

Effect of NP-Sia on Aβ Aggregation. After demonstrating Aβ can bind with NP-Sia, we assessed the effects of NP on Aβ aggregation and fibril growth via native gel electrophoresis. Native PAGE gels can preserve the fibrillar and protofibrillar integrity of Aβ and prevent the potential fibril deaggregation in the presence of detergent such as sodium dodecyl sulfate.[28] Aβ monomers were incubated with NP-Sia at 25 °C followed by native-PAGE gel electrophoresis. At room temperature, Aβ aggregation was slower with significant amounts of oligomers observed after 24 h (Figure 7, lane 1). With increasing concentrations of NP-Sia (0.02–2 mg/mL), the oligomers of

dx.doi.org/10.1021/cn3002015 | ACS Chem. Neurosci. 2013, 4, 575–584

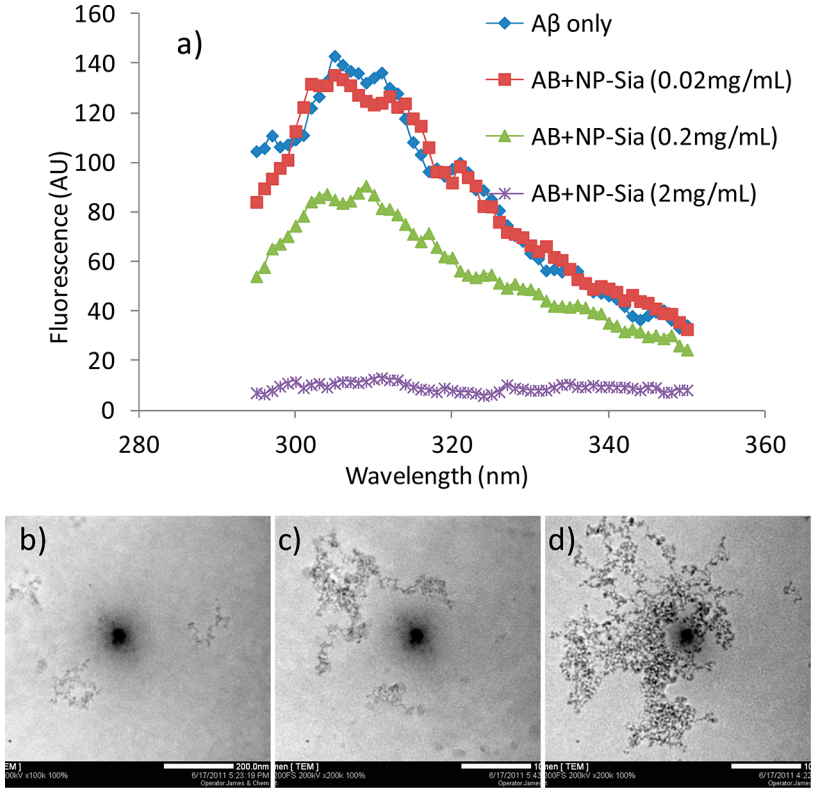

Figure 4. (a) Emission spectra of supernatants upon incubation of Aβ with NP-Sia followed by centrifugation (excitation wavelength 280 nm). TEM images of the pellets obtained by incubating Aβ with (b) 0.02 mg/mL, (c) 0.2 mg/mL, and (d) 2 mg/mL NP-Sia followed by centrifugation.

Aβ disappeared with concomitant increase in fibrils formed (lanes 2−4 of Figure 7, and Supporting Information Figure S5). This indicates that NP-Sia can reduce the amount of the Aβ oligomers in solution presumably by expediting the formation of Aβ fibrils.

NP-Sia effect on Aβ-Induced Cytotoxicity. For potential applications in Aβ detection and AD diagnosis, it is crucial that the contrast agents do not cause toxicities to the neuronal cells. To evaluate this, cell viability MTS assays were performed using SH-SY5Y neuroblastoma cells. The MTS assay is a colorimetric assay measuring the metabolic activities of mitochondria. Aβ exhibited significant cytotoxicities (Figure 8a) with an IC_{50} value of about 2 μM. NP-Sia (250 μg/mL) was found to be nontoxic to the cells, suggesting the high biocompatibility of the NPs. To confirm the MTS assay results, another cell viability assay, that is, LIVE/DEAD assay, was utilized. The LIVE/DEAD assay determines cell viability based on plasma membrane integrity and esterase activity, which is complementary to MTS. Consistent with the MTS assay results, the LIVE/DEAD assay gave similar IC_{50} values for Aβ induced cytotoxicity (Supporting Information Figure S6).

Although there is ongoing debate regarding the cause of AD, it is generally accepted that the aggregation state of Aβ is crucial in determining its degree of neurotoxicity and the soluble Aβ oligomeric form may be the key effectors of cytotoxicity in AD.[7,29] As NP-Sia can sequester Aβ and reduce the amounts of oligomers in solution, we envision that NP-Sia can potentially protect cells from Aβ induced cytotoxicities. To test this possibility, SH-SY5Y cells were treated with fixed concentration of Aβ (2 μM) in the presence of variable amounts of NP-Sia (0.0001, 0.001, 0.1, and 0.5 mg/mL). Without NP-Sia, approximately 50% of the cells remained viable after 24 h incubation. A dose dependent increase in cell viability was observed with increasing concentrations of NP-Sia in both MTS and LIVE/DEAD assays, where 0.5 mg/mL of NP-Sia was able to increase the viability of the cell cells to 80% (Figure 8b). This suggests that NP-Sia can mitigate the toxicity of Aβ, presumably by segregating Aβ in the fibril form on the NP. The full impact of NP-Sia and NP-Sia/Aβ complex on brain as well as the clearance of NP-Sia/Aβ complex in vivo will need to be established through further studies.

Compared to literature reports of Aβ molecular imaging,[9] our approach is unique in that we take advantage of the interactions between Aβ and carbohydrates, which have not been explored much for Aβ detection. While the results are promising, further studies are necessary to demonstrate the sensitivity and the selectivity of NP-Sia in transgenic mice and humans and compare with those of other probes.

For future Aβ plaque imaging in vivo, it will be crucial that the contrast agent can access the plaques in the brain. To bypass the blood brain barrier (BBB), contrast agents can be injected directly into the brain.[9d] A less invasive method is to administer the contrast agent in combination with agents such as mannitol to temporarily open up the tight junctions in the BBB.[9c] Alternatively, cell-penetrating peptides[30] can be immobilized onto the nanoparticles to facilitate crossing of the BBB.[31] With its large surface area, NP-Sia is amenable to further modification to enhance its ability to cross the BBB.

■ CONCLUSION

We demonstrated that glyconanoparticles could selectively bind Aβ. The protein free blocking was important in ELISA assays to avoid the nonspecific absorption Aβ to plates. The superparamagnetic nature of the glyconanoparticles enabled the

dx.doi.org/10.1021/cn3002015 | ACS Chem. Neurosci. 2013, 4, 575−584

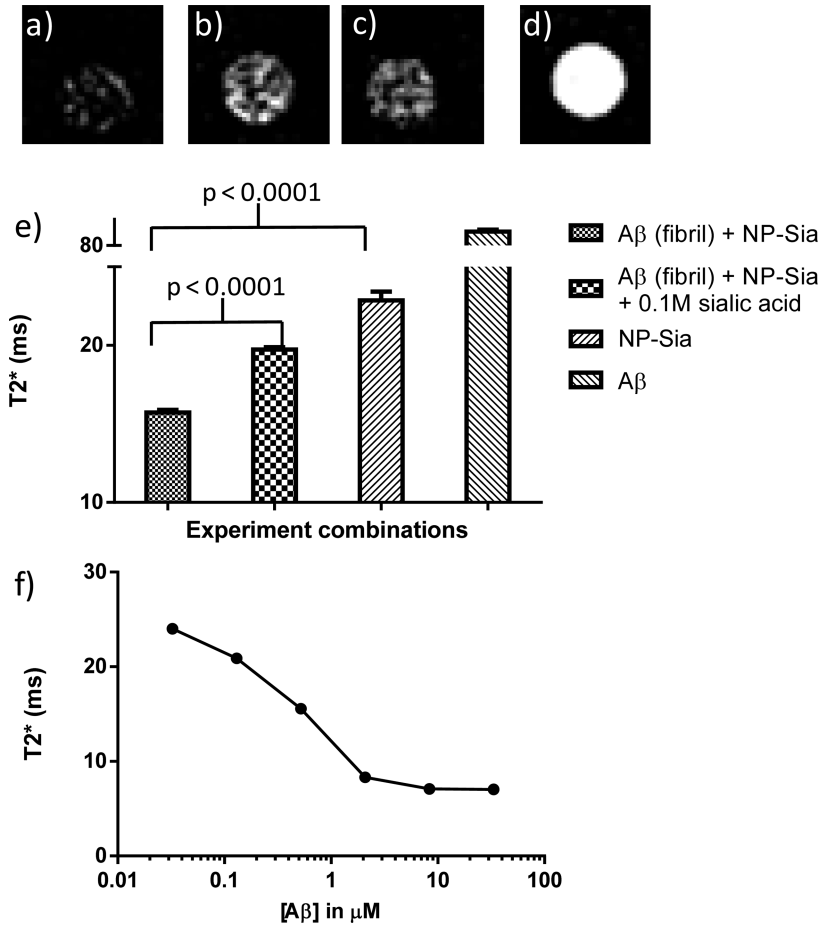

Figure 5. T2* weighted MR images of (a) NP-Sia (0.1 mg/mL) incubated with Aβ fibril (30 μM); (b) NP-Sia (0.1 mg/mL) incubated with Aβ fibril (30 μM) in the presence of free sialic acid (0.1 M); (c) NP-Sia (0.1 mg/mL); and (d) Aβ fibril (30 μM) only. (e) Quantification of T2* (ms) of images in (a)−(d). All error bars represent the standard deviation of three measurements. Statistical significances were obtained by *t* tests. (f) Changes of T2* relaxation time (ms) in the presence of increasing concentrations of Aβ.

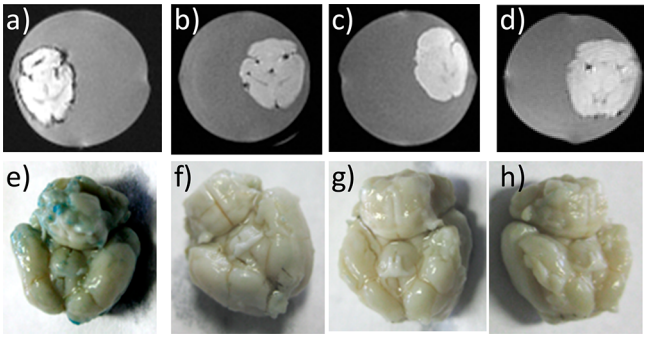

Figure 6. T2* weighted MR images of (a) Aβ mouse brain incubated with NP-Sia (0.1 mg/mL); (b) Aβ mouse brain incubated with NP-Sia (0.1 mg/mL) in the presence of free sialic acid (0.1 M); (c) normal mouse brain incubated with NP-Sia (0.1 mg/mL); and (d) Aβ mouse brain; Prussian blue staining of (e) Aβ mouse brain incubated with NP-Sia (0.1 mg/mL); (f) Aβ mouse brain incubated with NP-Sia (0.1 mg/mL) in the presence of free sialic acid (0.1 M); (g) normal mouse brain incubated with NP-Sia (0.1 mg/mL); and (h) Aβ mouse brain.

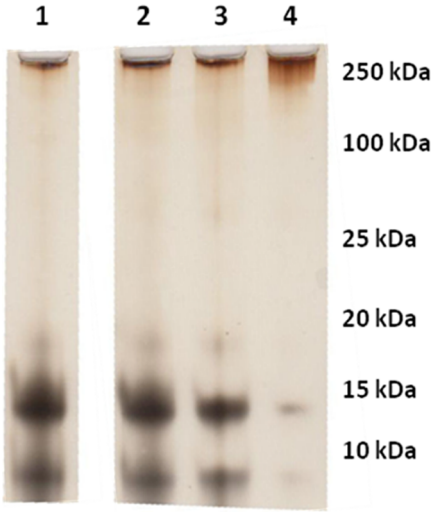

Figure 7. PAGE gel of Aβ. Aβ only (lane 1); Aβ incubated with 0.02 mg/mL (lane 2); 0.2 mg/mL (lane 3); and 2 mg/mL (lane 4) of NP-Sia.

detection of Aβ by MRI both in vitro and ex vivo on mouse brains. NP-Sia expedited the formation of Aβ fibril, thus converting Aβ to its less toxic form and protecting the cells from Aβ induced cytotoxicities. Other carbohydrates such as full structure of GM1 and glycosaminoglycans can be utilized to further enhance Aβ binding selectivity and specificity. These attributes coupled with the high biocompatibility, magnetic relaxivity and large surface area bode well for potential in vivo application of glyconanoparticles for Aβ detection and imaging.

dx.doi.org/10.1021/cn3002015 | *ACS Chem. Neurosci.* 2013, 4, 575−584

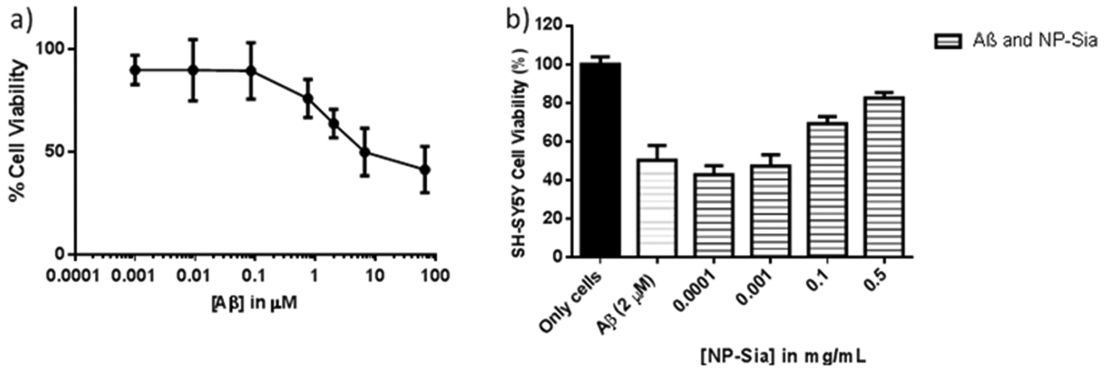

Figure 8. (a) Viability of SH-SY5Y neuroblastoma cells decreased with increasing concentration of Aβ as determined by MTS cell viability assay. (b) Addition of NP-Sia to SH-SY5Y neuroblastoma cells incubated with Aβ (2 μM) reduced Aβ induced cytotoxicity.

METHODS

Synthesis of NP-Sia. An aqueous solution of sialic acid **2**[18b] (100 mg, 0.208 mmol) and EDC (150 mg, 0.78 mmol) in water (10 mL) was stirred for 30 min at room temperature. NP-NH_2 (100 mg in 15 mL of pH 8.5 carbonate buffer) was added and stirred for 12 h at room temperature. The reaction mixture was centrifuged through 100 000 MWCO Amicon centrifugal filters. The supernatant was collected, and an aqueous solution of 0.01 M sodium hydroxide was added until the pH value reached 12. The reaction mixture was stirred at room temperature for 15 min, and the solution was neutralized by careful addition of 0.01 M hydrochloric acid. The reaction mixture was centrifuged through 100 000 MWCO Amicon centrifugal filters. The supernatant was diluted with water and centrifuged again. This process was repeated three times.

Deaggregation and Preparation of Aβ. Synthetic Aβ(1−42) peptide (1 mg) was dissolved in spectroscopy grade 99.9% 1,1,1,3,3,3-hexafluoro-2-propanol (3 mL), sonicated for 15 min, and lyophilized for 72 h. The thin peptide film was dissolved in 0.22 μm filtered solution of 10 mM NaOH solution (0.25 mL) followed by dilution with deionized water (0.625 mL) and PBS buffer (0.625 mL) to the desired final volume of 1.5 mL (the stock Aβ solution concentration is 147.7 μM). For experiments requiring fibril formation, the previous solution was incubated for 48 h at 37 °C.

ELISA Assay. To a well in a Nunc MaxiSorp 96-well ELISA plate was added 50 μL of NP-Sia solution (0.5 mg/mL), which was incubated at 37 °C overnight. After washing the wells with 3 × 300 mL PBST, 50 μL of Aβ solutions with various concentrations were added to the wells (0.34, 1.38, 5.53, 22.1, 88.5 μM) and incubated at 22 °C for 12 h. The plates were washed with 3 × 300 mL PBST and the anti-Aβ(1−16) IgG (6E10) monoclonal antibody, SIG-39320 (50 μL per well, 0.137nM, 1:24 000 in 1% (w/v) BSA containing PBS) was added, which in turn was incubated at 22 °C for 1 h. After washing with 3 × 300 μL PBST, the solution was discarded and the wells were washed three times with 300 μL of PBST and incubated for 1 h with 50 μL of the goat anti-mouse HRP-conjugated secondary antibody (1.7 nM, 1:18 000 in 1% (w/v) BSA in PBS). The solution was discarded, and the wells were washed three times with 300 μL of PBST. To a freshly prepared 3,3′,5,5′-tetramethylbenzidine (TMB) solution (5 mg of TMB was dissolved in 2 mL of DMSO and then diluted to 20 mL with citrate phosphate buffer), 20 μL of H_2O_2 was added. This mixture (150 μL) was immediately added to the ELISA wells. Blue color was allowed to develop for 10−20 min. The reaction was quenched (yellow color) by addition of 0.5 M H_2SO_4 (50 μL/well) and the absorbance was measured at 450 nm on an iMark microplate reader.

For sialic acid inhibition assay, a solution of NP-Sia (0.5 mg/mL, 50 μL) was incubated in a 96-well plate at 37 °C overnight. After washing the wells with PBST (3 × 300 μL), Aβ (0.5 μM, 50 μL) was added to the wells immediately followed addition 50 μL of different dilutions of pH 7.4 sialic acid solution (0.00048, 0.0019, 0.0078, 0.031, 0.125, 0.5 M). The plate was incubated at 22 °C for 12 h. The previous protocols were then followed for antibody incubation and color development.

Intrinsic Tyrosine Fluorescence Assay. An Aβ solution in 10 mM NaOH (443 μM, 13.5 μL) was added to a solution of NP-Sia with different concentrations 0.02, 0.2, and 2 mg/mL NP-Sia to a final volume of 200 μL in eppendorf tubes. The tubes were gently mixed and incubated at room temperature for 24 h. After incubation, the samples were centrifuged for 20 min at 10 000g to sediment fibrils and aggregates. The tyrosine fluorescence of the supernatant was measured via a HITACHI F-4500 fluorometer (excitation wavelength at 280 nm).

Aβ/NP-Sia Binding MRI Experiments. Six eppendorf tubes containing nanoparticles and Aβ were incubated in PBS buffer (total volume 750 μL) for 24 h at room temperature. The final concentration of NP-Sia was 0.33 mg/mL, and the final concentration for Aβ was 10 μM. For sialic acid competition experiments, free sialic acid (0.1 M) was added. The composition of the tubes was as follows: only Aβ, only NP-Sia, fibrillar Aβ+NP-Sia, fibrillar Aβ+NP-Sia+0.1 M free sialic acid, monomeric Aβ+NP-Sia, and monomeric Aβ+NP-Sia+0.1 M free sialic acid (each tube had a total volume of 750 μL in PBS buffer). Following incubation, 2% agarose gel (1.75 mL) was added to the incubated samples to make the final volume of 2.5 mL in 5 mL polystyrene round-bottom FACS tubes (BD Falcon). The tubes were placed at room temperature for 5 min and then at 4 °C until the time of MRI. To evaluate the T2* characteristics of the nanoparticles in phantoms, the following parameters were used: head coil, 3D fast spoiled gradient recalled echo sequence, flip angle = 15°, 16 echo times (TEs) = 2.1, 4.6, 7.0, 9.4, 11.8, 14.3, 16.7, 19.1, 21.5, 24.0, 26.4, 28.8, 31.2, 33.7, 36.1, and 38.5 ms, time of repetition = 41.9 ms, receiver bandwidth = ±62.5 kHz, field of view = 16 cm, slice thickness = 1.5 mm, number of slices = 16, acquisition matrix = 256 × 256, and number of excitation = 1.

Ex Vivo Brain Aβ/NP-Sia Binding MRI Experiments. The brains of C57BL6 mice were harvested and fixed in buffered 10% formalin solution for 48 h. After washing with deionized water, brains were incubated with 22 μM Aβ (4 mL) for 48 h at 4 °C. The Aβ treated brains were incubated with NP-Sia (0.6 mg/mL, 4 mL) for 24 h at 37 °C after washing with deionized water. After incubation, the brains were washed thoroughly and placed in a 6-well plate (Costar 3516, Corning) in water. For the sialic acid competition experiment, 0.1 M free sialic acid was added with NP-Sia (4 mL). The brains were imaged with the following parameters (T2* weighted sequence): wrist coil, 3D fast spoiled gradient recalled echo sequence, flip angle = 15°, echo times = 9.8 ms, time of repetition = 20 ms, receiver bandwidth = ±7.8 kHz, field of view = 8 cm, slice thickness = 0.5 mm, number of slices = 48, acquisition matrix = 256 × 256, and number of excitation = 3.

Prussian Blue Staining of Mice Brains. The same brains used in the ex vivo Aβ/NP-Sia MRI binding experiment were stained directly after imaging. Brains were soaked in 10% $K_4Fe[CN]_6$ solution, incubated for 10 min, and then transferred to a vial containing a mixture of 10 wt % $K_4Fe[CN]_6$/20 wt % HCl with a volume ratio of 1:1 for 10 min (Gomori's modified Prussian blue). The tissues were

dx.doi.org/10.1021/cn3002015 | ACS Chem. Neurosci. 2013, 4, 575−584

washed with water four times. A blue color was observed on the areas bearing iron oxide nanoparticles.

MTS Cytotoxicity Assay. SH-SY5Y cells were plated into 96-well plates at a density of 4×10^4 cells per well in 10% DMEM cell culture media for 24 h at 37 °C and 5% CO_2. The culture medium was replaced with 2% serum solution of different concentrations of Aβ (0.001. 0.0092, 0.085, 0.75, 2, 5.5, 66 μM, 100 μL/well). After 24 h incubation at 37 °C, the medium was replaced with MTS solution (20 μL in 200 μL) in culture medium and incubated for 6 h at 37 °C. The developed brown color in the wells was an indication of live cells. The absorption of the plate was measured at 490 nm in an iMark microplate reader (BioRad). Wells without cells (blanks) were subtracted as background from each sample. To test the effect of NP-Sia on Aβ induced cytotoxicity, cells were incubated with Aβ (2 μM). Various concentrations of NP-Sia (0.0001, 0.001, 0.1, and 0.5 mg/mL) were added. The cell viabilities were evaluated in a similar manner as described above.

■ ASSOCIATED CONTENT

Supporting Information

Additional experimental methods and procedures. This material is available free of charge via the Internet at http://pubs.acs.org.

■ AUTHOR INFORMATION

Corresponding Author

*Tel: +1-517-355-9715, ext 329. Fax: +1-517-353-1793. E-mail: xuefei@chemistry.msu.edu.

Present Address

[‖]M.H.E.-D.: Department of Chemistry, Beirut Arab University, Beirut, Lebanon.

Author Contributions

H.K. performed the majority of the experiments and participated in the experimental design and manuscript writing. D.C.Z. performed the MRI experiments and associated analysis. M.H.E.-D. performed the cell culture and initial LIVE/DEAD assay. K.L. synthesized the sialic acid ester. J.C. and W.L. performed the high resolution magic angle spinning NMR measurements. X.H. designed the experiments, oversaw the project, and wrote the manuscript.

Funding

We would like to thank the Department of Radiology, Michigan State University for the very generous support towards access of the MRI scanner and the National Institutes of Health (R01CA149451-01A1) for partial support of the nanoparticle synthesis and characterization efforts.

Notes

The authors declare no competing financial interest.

■ ACKNOWLEDGMENTS

We are grateful for the helpful suggestions from Prof. Jerry Yang (UCSD) towards our study.

■ REFERENCES

(1) Alzheimer's Association. Alzheimer's disease facts and figures. *Alzheimer's & Dementia*; Alzheimer Foundation: Washington, DC, 2011; Vol. 7.

(2) (a) Brookmeyer, R., Gray, S., and Kawas, C. (1998) Projections of Alzheimer's disease in the United States and the public health impact of delaying disease onset. *Am. J. Public Health 88*, 1337−1342. (b) Coreybloom, J., Thal, L. J., Galasko, D., Folstein, M., Drachman, D., Raskind, M., and Lanska, D. J. (1995) Diagnosis and evaluation of dementia. *Neurology 45*, 211−218. (c) Ostwald, S. K., Hepburn, K. W., Caron, W., Burns, T., and Mantell, R. (1999) Reducing caregiver burden: A randomized psychoeducational intervention for caregivers of persons with dementia. *Gerontologist 39*, 299−309. (d) Ernst, R. L., and Hay, J. W. (1994) The US economic and social cost of Alzheimers-disease revisited. *Am. J. Public Health 84*, 1261−1264. (e) Wimo, A., and Winblad, B. (2004) Economic aspects on drug therapy of dementia. *Curr. Pharm. Des. 10*, 295−301.

(3) (a) Minati, L., Grisoli, M., and Bruzzone, M. G. (2007) MR spectroscopy, functional MRI, and diffusion-tensor imaging in the aging brain: A conceptual review. *J. Geriatr. Psych. Neur. 20*, 3−21. (b) Lehericy, S., Marjanska, M., Mesrob, L., Sarazin, M., and Kinkingnehun, S. (2007) Magnetic resonance imaging of Alzheimer's disease. *Eur. Radiol. 17*, 347−362. (c) Sandson, T. A., Oconnor, M., Sperling, R. A., Edelman, R. R., and Warach, S. (1996) Noninvasive perfusion MRI in Alzheimer's disease: A preliminary report. *Neurology 47*, 1339−1342. (d) Alsop, D. C., Detre, J. A., and Grossman, M. (2000) Assessment of cerebral blood flow in Alzheimer's disease by spin-labeled magnetic resonance imaging. *Ann. Neurol. 47*, 93−100.

(4) (a) De Santi, S., de Leon, M. J., Rusinek, H., Convit, A., Tarshish, C. Y., Roche, A., Tsui, W. H., Kandil, E., Boppana, M., Daisley, K., Wang, G. J., Schlyer, D., and Fowler, J. (2001) Hippocampal formation glucose metabolism and volume losses in MCI and AD. *Neurobiol. Aging 22*, 529−539. (b) Colloby, S. J., Fenwick, J. D., Williams, E. D., Paling, S. M., Lobotesis, K., Ballard, C., McKeith, I., and O'Brien, J. T. (2002) A comparison of Tc-99m-HMPAO SPET changes in dementia with Lewy bodies and Alzheimer's disease using statistical parametric mapping. *Eur. J. Nucl. Med. Mol. Imaging 29*, 615−622. (c) Bonte, F. J., Harris, T. S., Roney, C. A., and Hynan, L. S. (2004) Differential diagnosis between Alzheimer's and frontotemporal disease by the posterior cingulate sign. *J. Nucl. Med. 45*, 771−774. (d) Caroli, A., Testa, C., Geroldi, C., Nobili, F., Barnden, L. R., Guerra, U. P., Bonetti, M., and Frisoni, G. B. (2007) Cerebral perfusion correlates of conversion to Alzheimer's disease in amnestic mild cognitive impairment. *J. Neurol. 254*, 1698−1707. (e) Mosconi, L., Tsui, W. H., De Santi, S., Li, J., Rusinek, H., Convit, A., Li, Y., Boppana, M., and de Leon, M. J. (2005) Reduced hippocampal metabolism in MCI and AD - automated FDG-PET image analysis. *Neurology 64*, 1860−1867.

(5) (a) Hardy, J. A., and Higgins, G. A. (1992) Alzheimers-disease - The Amyloid Cascade Hypothesis. *Science 256*, 184−185. (b) Selkoe, D. J. (1994) Alzheimers-disease - A central role for amyloid. *J. Neuropathol. Exp. Neurol. 53*, 438−447.

(6) Hartmann, T., Bieger, S. C., Bruhl, B., Tienari, P. J., Ida, N., Allsop, D., Roberts, G. W., Masters, C. L., Dotti, C. G., Unsicker, K., and Beyreuther, K. (1997) Distinct sites of intracellular production for Alzheimer's disease A beta 40/42 amyloid peptides. *Nat. Med. 3*, 1016−1020.

(7) Bitan, G., Vollers, S. S., and Teplow, D. B. (2003) Elucidation of primary structure elements controlling early amyloid beta-protein oligomerization. *J. Biol. Chem. 278*, 34882−34889.

(8) (a) Klunk, W. E., Engler, H., Nordberg, A., Wang, Y. M., Blomqvist, G., Holt, D. P., Bergstrom, M., Savitcheva, I., Huang, G. F., Estrada, S., Ausen, B., Debnath, M. L., Barletta, J., Price, J. C., Sandell, J., Lopresti, B. J., Wall, A., Koivisto, P., Antoni, G., Mathis, C. A., and Langstrom, B. (2004) Imaging brain amyloid in Alzheimer's disease with Pittsburgh compound-B. *Ann. Neurol. 55*, 306−319. (b) Van-broeckhoven, C., Haan, J., Bakker, E., Hardy, J. A., Vanhul, W., Wehnert, A., Vegtervandervlis, M., and Roos, R. A. C. (1990) Amyloid-beta protein-precursor gene and hereditary cerebral-hemorrhage with amyloidosis (Dutch). *Science 248*, 1120−1122. (c) Shoghi-Jadid, K., Small, G. W., Agdeppa, E. D., Kepe, V., Ercoli, L. M., Siddarth, P., Read, S., Satyamurthy, N., Petric, A., Huang, S. C., and Barrio, J. R. (2002) Localization of neurofibrillary tangles and beta-amyloid plaques in the brains of living patients with Alzheimer disease. *Am. J. Geriat. Psychiatry 10*, 24−35. (d) Rowe, C. C., Ackerman, U., Browne, W., Mulligan, R., Pike, K. L., O'Keefe, G., Tochon-Danguy, H., Chan, G., Berlangieri, S. U., Jones, G., Dickinson-Rowe, K. L., Kung, H. P., Zhang, W., Kung, M. P., Skovronsky, D., Dyrks, T., Hall, G., Krause, S., Friebe, M., Lehman, L., Lindemann, S., Dinkelborg, L. M., Masters, C. L., and Villemagne, V. L. (2008) Imaging of amyloid beta in Alzheimer's disease with F-18-BAY94−9172, a novel PET tracer: proof of mechanism. *Lancet Neurol. 7*, 129−135. (e) Barthel, H.,

Gertz, H.-J., Dresel, S., Peters, O., Bartenstein, P., Buerger, K., Hiemeyer, F., Wittemer-Rump, S. M., Seibyl, J., Reininger, C., Sabri, O., and Florbetaben Study, G. (2011) Cerebral amyloid-beta PET with Florbetaben (F-18) in patients with Alzheimer's disease and healthy controls: A multicentre phase 2 diagnostic study. *Lancet Neurol. 10*, 424−435. (f) Villemagne, V. L., Ong, K., Mulligan, R. S., Holl, G., Pejoska, S., Jones, G., O'Keefe, G., Ackerman, U., Tochon-Danguy, H., Chan, J. G., Reininger, C. B., Fels, L., Putz, B., Rohde, B., Masters, C. L., and Rowe, C. C. (2011) Amyloid imaging with F-18-Florbetaben in Alzheimer disease and other dementias. *J. Nucl. Med. 52*, 1210−1217. (g) Wong, D. F., Rosenberg, P. B., Zhou, Y., Kumar, A., Raymont, V., Ravert, H. T., Dannals, R. F., Nandi, A., Brasic, J. R., Ye, W., Hilton, J., Lyketsos, C., Kung, H. F., Joshi, A. D., Skovronsky, D. M., and Pontecorvo, M. J. (2010) In vivo imaging of amyloid deposition in Alzheimer disease using the radioligand F-18-AV-45 (Flobetapir F 18). *J. Nucl. Med. 51*, 913−920. (h) Clark, C. M., Schneider, J. A., Bedell, B. J., Beach, T. G., Bilker, W. B., Mintun, M. A., Pontecorvo, M. J., Hefti, F., Carpenter, A. P., Flitter, M. L., Krautkramer, M. J., Kung, H. F., Coleman, R. E., Doraiswamy, P. M., Fleisher, A. S., Sabbagh, M. N., Sadowsky, C. H., Reiman, P. E. M., Zehntner, S. P., Skovronsky, D. M., and Grp, A. A. S. (2011) Use of Florbetapir-PET for imaging beta-amyloid pathology. *JAMA, J. Am. Med. Assoc. 305*, 275−283.

(9) (a) Siegemund, T., Paulke, B. R., Schmiedel, H., Bordag, N., Hoffmann, A., Harkany, T., Tanila, H., Kacza, J., and Hartig, W. (2006) Thioflavins released from nanoparticles target fibrillar amyloid beta in the hippocampus of APP/PS1 transgenic mice. *Int. J. Dev. Neurosci. 24*, 195−201. (b) Poduslo, J. F., Wengenack, T. M., Curran, G. L., Wisniewski, T., Sigurdsson, E. M., Macura, S. I., Borowski, B. J., and Jack, C. R. (2002) Molecular targeting of Alzheimer's amyloid plaques for contrast-enhanced magnetic resonance imaging. *Neurobiol. Dis. 11*, 315−329. (c) Wadghiri, Y. Z., Sigurdsson, E. M., Sadowski, M., Elliott, J. I., Li, Y. S., Scholtzova, H., Tang, C. Y., Aguinaldo, G., Pappolla, M., Duff, K., Wisniewski, T., and Turnbull, D. H. (2003) Detection of Alzheimer's amyloid in transgenic mice using magnetic resonance microimaging. *Magn. Reson. Med. 50*, 293−302. (d) Petiet, A., Santina, M., Bertrand, A., Wiggins, C. J., Petit, F., Houitte, D., Hantraye, P., Benavides, J., Debeir, T., Rooney, T., and Dhenain, M. (2012) Gadolinium-staining reveals amyloid plaques in the brain of Alzheimer's transgenic mice. *Neurobiol. Aging 33*, 1533−1544. (e) Higuchi, M., Iwata, N., Matsuba, Y., Sato, K., Sasamoto, K., and Saido, T. C. (2005) ^{19}F and ^{1}H MRI detection of amyloid beta plaques in vivo. *Nat. Neurosci. 8*, 527−533.

(10) Hintersteiner, M., Enz, A., Frey, P., Jaton, A.-L., Kinzy, W., Kneuer, R., Neumann, U., Rudin, M., Staufenbiel, M., Stoeckli, M., Wiederhold, K.-H., and Gremlich, H.-U. (2005) In vivo detection of amyloid-β deposits by near-infrared imaging using an oxazine-derivative probe. *Nat. Biotechnol. 23*, 577−583.

(11) (a) Di Domizio, J., Zhang, R., Stagg, L. J., Gagea, M., Zhuo, M., Ladbury, J. E., and Cao, W. (2012) Binding with nucleic acids or glycosaminoglycans converts soluble protein oligomers to amyloid. *J. Biol. Chem. 287*, 736−747. (b) Braun, S., Humphreys, C., Fraser, E., Brancale, A., Bochtler, M., and Dale, T. C. (2011) Amyloid-associated nucleic acid hybridisation. *PLoS One 6*, e19125.

(12) (a) Yanagisawa, K., Odaka, A., Suzuki, N., and Ihara, Y. (1995) GM1 ganglioside-bound amyloid beta-protein (Abeta): A possible form of preamyloid in alzheimer's disease. *Nat. Med. 1*, 1062−1066. (b) Ariga, T., and Yu, R. K. (1999) GM1 Inhibits amyloid beta-protein-induced cytokine release. *Neurochem. Res. 24*, 219−226. (c) Wakabayashi, M., Okada, T., Kozutsumi, Y., and Matsuzaki, K. (2005) GM1 ganglioside-mediated accumulation of amyloid beta-protein on cell membranes. *Biochem. Biophys. Res. Commun. 328*, 1019−1023.

(13) Nagai, Y. (1995) Functional roles of gangliosides in bio-signaling. *Behav. Brain Res. 66*, 99−104.

(14) Williamson, M. P., Suzuki, Y., Bourne, N. T., and Asakura, T. (2006) Binding of amyloid beta-peptide to ganglioside micelles is dependent on histidine-13. *Biochem. J. 397*, 483−490.

(15) (a) Kakio, A., Nishimoto, S., Yanagisawa, K., Kozutsumi, Y., and Matsuzaki, K. (2001) Cholesterol-dependent formation of GM1 ganglioside-bound amyloid beta-protein, an endogenous seed for Alzheimer amyloid. *J. Biol. Chem. 276*, 24985−24990. (b) Kakio, A., Yano, Y., Takai, D., Kuroda, Y., Matsumoto, O., Kozutsumi, Y., and Matsuzaki, K. (2004) Interaction between amyloid beta-protein aggregates and membranes. *J. Pept. Sci. 10*, 612−621. (c) Yamamoto, N., Matsubara, T., Sato, T., and Yanagisawa, K. (2009) Age-dependent high-density clustering of GM1 ganglioside at presynaptic neuritic terminals promotes amyloid β-protein fibrillogenesis. *Biochim. Biophys. Acta 1778*, 2717−2726. (d) Patel, D., Henry, J., and Good, T. (2006) Attenuation of beta-amyloid induced toxicity by sialic acid-conjugated dendrimeric polymers. *Biochim. Biophys. Acta, Gen. Subj. 1760*, 1802−1809. (e) Cowan, C. B., Cote, G. L., and Good, T. A. (2008) Development of photocrosslinked sialic acid containing polymers for use in Abeta toxicity attenuation. *Biomaterials 29*, 3408−3414. (f) Patel, D. A., Henry, J. E., and Good, T. A. (2007) Attenuation of beta-amyloid-induced toxicity by sialic-acid-conjugated dendrimers: Role of sialic acid attachment. *Brain Res. 1161*, 95−105.

(16) (a) Barnham, K. J., Kenche, V. B., Ciccotosto, G. D., Smith, D. P., Tew, D. J., Liu, X., Perez, K., Cranston, G. A., Johanssen, T. J., Volitakis, I., Bush, A. I., Masters, C. L., White, A. R., Smith, J. P., Cherny, R. A., and Cappai, R. (2008) Platinum-based inhibitors of amyloid-beta as therapeutic agents for Alzheimer's disease. *Proc. Natl. Acad. Sci. U.S.A. 105*, 6813−6818. (b) Kim, J. E., and Lee, M. (2003) Fullerene inhibits beta-amyloid peptide aggregation. *Biochem. Bioph. Res. Co. 303*, 576−579. (c) Ikeda, K., Okada, T., Sawada, S.-i., Akiyoshi, K., and Matsuzaki, K. (2006) Inhibition of the formation of amyloid beta-protein fibrils using biocompatible nanogels as artificial chaperones. *FEBS Lett. 580*, 6587−6595. (d) Geng, J., Li, M., Ren, J., Wang, E., and Qu, X. (2011) Polyoxometalates as inhibitors of the aggregation of amyloid beta peptides associated with Alzheimer's disease. *Angew. Chem., Int. Ed. 50*, 4184−4188. (e) Yoo, S. I., Yang, M., Brender, J. R., Subramanian, V., Sun, K., Joo, N. E., Jeong, S.-H., Ramamoorthy, A., and Kotov, N. A. (2011) Inhibition of amyloid peptide fibrillation by inorganic nanoparticles: Functional similarities with proteins. *Angew. Chem., Int. Ed. 50*, 5110−5115. (f) Saraiva, A. M., Cardoso, I., Carmo Pereira, M., Coelho, M. A. N., Joao Saraiva, M., Moehwald, H., and Brezesinski, G. (2010) Controlling amyloid-beta peptide(1−42) oligomerization and toxicity by fluorinated nanoparticles. *ChemBioChem 11*, 1905−1913. (g) Zhang, D., Neumann, O., Wang, H., Yuwono, V. M., Barhoumi, A., Perham, M., Hartgerink, J. D., Wittung-Stafshede, P., and Halas, N. J. (2009) Gold nanoparticles can induce the formation of protein-based aggregates at physiological pH. *Nano Lett. 9*, 666−671. (h) Rocha, S., Thueneman, A. F., Pereira, M. d. C., Coelho, M., Moehwald, H., and Brezesinski, G. (2008) Influence of fluorinated and hydrogenated nanoparticles on the structure and fibrillogenesis of amyloid beta-peptide. *Biophys. Chem. 137*, 35−42. (i) Bieschke, J., Herbst, M., Wiglenda, T., Friedrich, R. P., Boeddrich, A., Schiele, F., Kleckers, D., del Amo, J. M. L., Gruening, B. A., Wang, Q., Schmidt, M. R., Lurz, R., Anwyl, R., Schnoegl, S., Faendrich, M., Frank, R. F., Reif, B., Guenther, S., Walsh, D. M., and Wanker, E. E. (2012) Small-molecule conversion of toxic oligomers to nontoxic beta-sheet-rich amyloid fibrils. *Nat. Chem. Biol. 8*, 93−101. (j) Wu, W.-h., Sun, X., Yu, Y.-p., Hu, J., Zhao, L., Liu, Q., Zhao, Y.-f., and Li, Y.-m. (2008) TiO_2 nanoparticles promote beta-amyloid fibrillation in vitro. *Biochem. Biophys. Res. Commun. 373*, 315−318. (k) Xiao, L., Zhao, D., Chan, W.-H., Choi, M. M. F., and Li, H.-W. (2010) Inhibition of beta 1−40 amyloid fibrillation with *N*-acetyl-L-cysteine capped quantum dots. *Biomaterials 31*, 91−98. (l) Brambilla, D., Verpillot, R., Le Droumaguet, B., Nicolas, J., Taverna, M., Kóňa, J., Lettiero, B., Hashemi, S. H., De Kimpe, L., Canovi, M., Gobbi, M., Nicolas, V., Scheper, W., Moghimi, S. M., Tvaroška, I., Couvreur, P., and Andrieux, K. (2012) PEGylated nanoparticles bind to and alter amyloid-beta peptide conformation: Toward engineering of functional nanomedicines for Alzheimer's disease. *ACS Nano 6*, 5897−5908.

(17) (a) Palmacci, S., Josephson, L., and Groman, E. Synthesis of polysaccharide covered superparamagnetic oxide colloids, U.S. Patent 9505669, 1995. (b) El-Dakdouki, M. H., Zhu, D. C., El-boubbou, K., Kamat, M., Chen, J., Li, W., and Huang, X. (2012) Development of multifunctional hyaluronan-coated nanoparticles for imaging and drug

delivery to cancer cells. *Biomacromolecules 13*, 1144−1151. (c) Kamat, M., El-boubbou, K., Zhu, D., Lansdell, T., Lu, X., Li, W., and Huang, X. (2010) Hyaluronic acid immobilized magnetic nanoparticles for active targeting and imaging of macrophages. *Bioconjugate Chem. 21*, 2128−2135.

(18) (a) El-Boubbou, K., Zhu, D. C., Vasileiou, C., Borhan, B., Prosperi, D., Li, W., and Huang, X. (2010) Magnetic glyco-nanoparticles: A tool to detect, differentiate, and unlock the glyco-codes of cancer via magnetic resonance imaging. *J. Am. Chem. Soc. 132*, 4490−4499. (b) Wang, Y., El-Boubbou, K., Kouyoumdjian, H., Sun, B., Huang, X., and Zeng, X. (2010) Lipoic acid glyco-conjugates, a new class of agents for controlling nonspecific adsorption of blood serum at biointerfaces for biosensor and biomedical applications. *Langmuir 26*, 4119−4125.

(19) Roher, A. E., Lowenson, J. D., Clarke, S., Woods, A. S., Cotter, R. J., Gowing, E., and Ball, M. J. (1993) Beta-amyloid-(1−42) is a major component of cerebrovascular amyloid deposits: Implications for the pathology of Alzheimer disease. *Proc. Natl. Acad. Sci. U.S.A. 90*, 10836−10840.

(20) (a) García-Matas, S., de Vera, N., Aznar, A. O., Marimon, J. M., Adell, A., Planas, A. M., Cristòfol, R., and Sanfeliu, C. (2010) In vitro and in vivo activation of astrocytes by amyloid-beta is potentiated by pro-oxidant agents. *J. Alzheimer's Dis. 20*, 229−245. (b) Allaman, I., Gavillet, M., Bélanger, M., Laroche, T., Viertl, D., Lashuel, H. A., and Magistretti, P. J. (2010) Amyloid-beta aggregates cause alterations of astrocytic metabolic phenotype: impact on neuronal viability. *J. Neurosci. 30*, 3326−3338.

(21) LeVine, H. (1999) Quantification of β-sheet amyloid fibril structures with Thioflavin T. *Methods Enzymol. 309*, 274−284.

(22) Khurana, R., Coleman, C., Ionescu-Zanetti, C., Carter, S. A., Krishna, V., Grover, R. K., Roy, R., and Singh, S. (2005) Mechanism of Thioflavin T binding to amyloid fibrils. *J. Struct. Biol. 151*, 229−238.

(23) Moores, B., Drolle, E., Attwood, S. J., Simons, J., and Leonenko, Z. (2011) Effect of surfaces on amyloid fibril formation. *PLoS One 6*, e25954.

(24) (a) Inbar, P., Bautista, M. R., Takayama, S. A., and Yang, J. (2008) Assay to screen for molecules that associate with Alzheimer's related beta-amyloid fibrils. *Anal. Chem. 80*, 3502−3506. (b) Inbar, P., and Yang, J. (2006) Inhibiting protein-amyloid interactions with small molecules: A surface chemistry approach. *Bioorg. Med. Chem. Lett. 16*, 1076−1079. (c) Inbar, P., Li, C. Q., Takayama, S. A., Bautista, M. R., and Yang, J. (2006) Oligo(ethylene glycol) derivatives of Thioflavin T as inhibitors of protein-amyloid interactions. *ChemBioChem 7*, 1563−1566. (d) Fraser, P. E., Darabie, A. A., and McLaurin, J. (2001) Amyloid-beta interactions with chondroitin sulfate-derived mono-saccharides and disaccharides - Implications for drug development. *J. Biol. Chem. 276*, 6412−6419.

(25) Bohrmann, B., Tjernberg, L., Kuner, P., Poli, S., Levet-Trafit, B., Naslund, J., Richards, G., Huber, W., Dobeli, H., and Nordstedt, C. (1999) Endogenous proteins controlling amyloid beta-peptide polymerization - Possible implications for beta-amyloid formation in the central nervous system and in peripheral tissues. *J. Biol. Chem. 274*, 15990−15995.

(26) (a) Jun, Y. W., Lee, J. H., and Cheon, J. (2008) Chemical design of nanoparticle probes for high-performance magnetic resonance imaging. *Angew. Chem., Int. Ed. 47*, 5122−5135. (b) Na, H. B., Song, I. C., and Hyeon, T. (2009) Inorganic nanoparticles for MRI contrast agents. *Adv. Mater. 21*, 2133−2148.

(27) (a) Roch, A., Gossuin, Y., Muller, R. N., and Gillis, P. (2005) Superparamagnetic colloid suspensions: Water magnetic relaxation and clustering. *J. Magn. Magn. Mater. 293*, 532−539. (b) Yung, K. T. (2003) Empirical models of transverse relaxation for spherical magnetic perturbers. *Magn. Reson. Imaging 21*, 451−463. (c) Lee, H., Sun, E., Ham, D., and Weissleder, R. (2008) Chip-NMR biosensor for detection and molecular analysis of cells. *Nat. Med. 14*, 869−874. (d) Koh, I., Hong, R., Weissleder, R., and Josephson, L. (2008) Sensitive NMR sensors detect antibodies to influenza. *Angew. Chem., Int. Ed. 47*, 4119−4121.

(28) Walsh, D., Lomakin, A., Benedek, G., Condron, M., and Teplow, D. (1997) Amyloid β-protein fibrillogenesis: Detection of a protofibrillar intermediate. *J. Biol. Chem. 272*, 22364−22372.

(29) (a) Bravo, R., Arimon, M., Valle-Delgado, J. J., García, R., Durany, N., Castel, S., Cruz, M., Ventura, S., and Fernàndez-Busquets, X. (2008) Sulfated polysaccharides promote the assembly of amyloid beta(1−42) peptide into stable fibrils of reduced cytotoxicity. *J. Biol. Chem. 283*, 32471−32483. (b) Teplow, D. B. Amyloid, Prions, and Other Protein Aggregates, Part C. In *Methods in Enzymology*; Academic Press: San Diego, 2006; Vol. 413, pp 20−33. (c) Bitan, G., and Teplow, D. B. (2005) Preparation of aggregate-free, low molecular weight amyloid-beta for assembly and toxicity assays. *Methods Mol. Biol. 299*, 3−9. (d) Lesne, S., Koh, M. T., Kotilinek, L., Kayed, R., Glabe, C. G., Yang, A., Gallagher, M., and Ashe, K. H. (2006) A specific amyloid-beta protein assembly in the brain impairs memory. *Nature 440*, 352−357. (e) Shankar, G. M., Li, S., Mehta, T. H., Garcia-Munoz, A., Shepardson, N. E., Smith, I., Brett, F. M., Farrell, M. A., Rowan, M. J., Lemere, C. A., Regan, C. M., Walsh, D. M., Sabatini, B. L., and Selkoe, D. J. (2008) Amyloid-beta protein dimers isolated directly from Alzheimer's brains impair synaptic plasticity and memory. *Nat. Med. 14*, 837−842. (f) Klein, W. L., Krafft, G. A., and Finch, C. E. (2001) Targeting small Abeta oligomers: the solution to an Alzheimer's disease conundrum? *Trends Neurosci. 24*, 219−224.

(30) Temsamani, J., and Vidal, P. (2004) The use of cell-penetrating peptides for drug delivery. *Drug Discovery Today 9*, 1012−1019.

(31) Silva, G. A. (2008) Nanotechnology approaches to crossing the blood-brain barrier and drug delivery to the CNS. *BMC Neurosci. 9* (Suppl 3), S4.